ACS EARTH AND SPACE CHEMISTRY

http://pubs.acs.org/journal/aesccq

Article

Redox Behavior of Cu onto Magnetite Nanoparticles

Jaimy SCARIA, Mathieu PÉDROT, Laura FABLET, Fadi CHOUEIKANI, Anne-Catherine PIERSON-WICKMANN, Aline DIA, Yann SIVRY, Charlotte CATROUILLET, and Rémi MARSAC*

Cite This: *ACS Earth Space Chem.* 2026, 10, 507−514

Read Online

ACCESS | Metrics & More | Article Recommendations | Supporting Information

ABSTRACT: Copper (Cu) oxidation-state distribution controls its toxicity and mobility in natural systems and is affected by its interaction with redox-reactive mineral surfaces such as magnetite. By combining aqueous chemical analysis, X-ray absorption spectroscopy and aqueous speciation modeling, this study provides detailed mechanistic insights regarding Cu redox speciation in solution and at the surface of 10 nm-sized magnetite nanoparticles with varying stoichiometries ($0.1 \leq R = Fe(II)/Fe(III) \leq 0.5$), versus pH (4 to 9) and initial Cu(II) concentration ($[Cu(II)]_{ini}$ = 25 and 500 μM), with 10 mM NaCl. Cu(II) generally prevailed at the magnetite surface, with co-occurring Cu(I) from a smaller extent to an equal extent. Conversely, in the aqueous solution (i.e., after filtration), Cu(I) prevailed at pH > 5, hence evidencing that solution and surface redox speciation may differ. Reduction to Cu(0) was only partial and detected under the most reducing condition (for R = 0.5) at high $[Cu(II)]_{ini}$, because it was limited by Cu(II)- and Cu(I)-magnetite binding. Significant oxidation Fe(II) to Fe(III) was shown to be responsible for this partial reduction process, which could be overcome by adding Fe(II) ions to recharge the magnetite surface, hence promoting further copper reduction to Cu(0). This study provides fundamental insights into copper−magnetite interactions and enables improved predictions of copper speciation and fate in environmental systems.

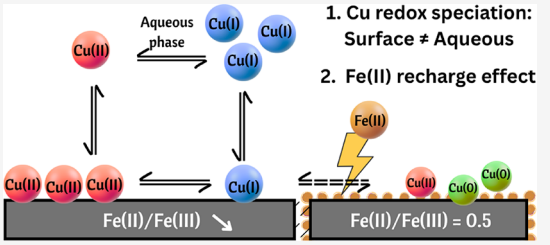

KEYWORDS: *magnetite, copper, speciation, redox, surface, X-ray absorption spectroscopy*

INTRODUCTION

Copper (Cu) occurs at trace levels in natural systems, with a complex biogeochemical cycle characterized by its multiple valence states (Cu(II), Cu(I), and Cu(0)) and dynamic interactions with biological and geological systems.[1] While Cu(II) is essential for metabolic processes, elevated Cu(II) concentrations may be harmful for living organisms. In addition, the oxidation state of Cu dictates its toxicity, because Cu(I) is much more toxic than Cu(II).[2,3] Iron-bearing minerals, which dominate redox processes in anoxic and suboxic environments, exert primary control over Cu fate and transport through surface-mediated electron transfer reactions.[4,5] Fe(III)-oxide minerals such as goethite (α-FeOOH), hematite (α-Fe_2O_3), and lepidocrocite (γ-FeOOH) exhibit limited reductive capacity, predominantly stabilizing Cu(II) as surface complexes without significant transformation.[6,7] Some Fe(II)-bearing minerals demonstrate substantial Cu(II) reduction: pyrite (FeS_2) reduces Cu(II) to Cu(I) independent of pH,[8,9] while Fe(II)-rich smectite and green rust are capable of fully reducing Cu(II) to Cu(0).[10,11] In the case of magnetite ($Fe(II)Fe(III)_2O_4$), the situation is unclear as preliminary evidence suggests Cu(II) reduction to Cu(I) or Cu(0),[12,13] but the lack of systematic investigation across environmental conditions prevents reliable prediction of Cu speciation in magnetite-bearing systems.

Magnetite is both abundant in anoxic environments and exhibits high Cu sorption capacity,[14] making it environmentally relevant for Cu transformations. Additionally, its tunable stoichiometry (R = Fe(II)/Fe(III)), which directly controls suspension redox potential (Eh), makes it an ideal model system for investigating Fe(II)-mediated Cu(II) reduction mechanisms.[15,16] The stoichiometry ranges from 0.5 in stoichiometric magnetite to 0 in fully oxidized maghemite, with natural systems typically exhibiting intermediate values ($0 \leq R \leq 0.5$).[17,18] The magnetite stoichiometry controls reductive transformations of various trace elements and radionuclides, including U(VI), Cr(VI), Re(VII), or V(V),[18−21] as well as organic contaminants.[14] By analogy, Cu(II) reduction to either Cu(I) or Cu(0) might depend on the magnetite stoichiometry, which in turn is controlled by the prevailing redox, pH, (geo)chemical conditions, and microbial activity in the environment.[22−24]

Received: October 16, 2025
Revised: January 21, 2026
Accepted: January 22, 2026
Published: January 29, 2026

This study investigates Cu-magnetite interaction mechanisms across controlled stoichiometries ($0.1 \leq R \leq 0.5$), initial Cu(II) concentrations (25−500 μM), and pH conditions (4−9). By coupling advanced spectroscopic techniques, X-ray absorption spectroscopy (XAS) at Cu $L_{2,3}$-edges and X-ray magnetic circular dichroism (XMCD) at Fe $L_{2,3}$-edges, with comprehensive solution-phase analyses under rigorous anaerobic conditions, this work quantifies coupled Fe(II) oxidation to Fe(III) and Cu(II) reduction to Cu(I) or Cu(0) at the magnetite surface. Because Cu(I) is substantially more toxic and bioavailable than Cu(II), these mechanistic insights are essential for predicting Cu environmental fate and ecotoxicological impacts in Fe(II)-rich systems commonly found in subsurface environments.

EXPERIMENTAL SECTION

Chemicals

Iron(III) chloride hexahydrate ($FeCl_3{\cdot}6H_2O$; 98−102%), iron(II) chloride tetrahydrate ($FeCl_2{\cdot}4H_2O \geq 99\%$), copper chloride ($CuCl_2{\cdot}6H_2O$; 95%) and hydrogen peroxide (H_2O_2), hydrochloric acid (HCl ≥ 37%), sulfuric acid (H_2SO_4; 95−97%) sodium hydroxide (NaOH ; 98%), 1−10-phenanthroline monohydrate (97%), and hydroxylamine hydrochloride were obtained from Sigma-Aldrich. Sodium chloride (NaCl) was purchased from Avantor Rectapur. Nitric acid (HNO_3) received from Sigma-Aldrich was extrapurified for ICP-MS analysis. All other chemicals are of analytical grade or better and used directly without additional purification. All solutions and standards were prepared with the Milli-Q-Gradient ultrapure water (Millipore, Merck Darmstadt, Germany specific resistivity 18.2 MΩ cm). All the experiments were performed in an anaerobic chamber (N_2-glovebox, JACOMEX, $O_{2(g)} < 1$ ppm), and all the solutions were purged with $N_{2(g)}$ for at least 12 h before use. The pH of all the samples was also adjusted by HCl and NaOH (no buffer was used).

Synthesis and Characterization of Magnetite Nanoparticles

The synthesis procedure involved chemical coprecipitation at room temperature under anaerobic conditions, according to a previously reported method.[17,25] Stoichiometric magnetite (R0.5) was synthesized and characterized from iron chloride salts (0.5 M $FeCl_2{\cdot}4H_2O$ and 1 M $FeCl_3{\cdot}6H_2O$) added in a 1:2 Fe(II)/Fe(III) proportion. The salts were dissolved in 0.5 M HCl solution and added dropwise into 250 mL of 0.5 M NaOH solution with continuous stirring, leading to an instantaneous precipitation of ∼10 nm average-sized magnetite nanoparticles at pH 8. The resulting mineral suspension was magnetically separated and three times washed with ultrapure water adjusted to pH 8 using NaOH, to avoid Fe(II) release.[22] Partially oxidized magnetite nanoparticles (R0.4, R0.3, R0.2, and R0.1) were made by adding known amounts of hydrogen peroxide (approximately 30% H_2O_2) to R0.5,[17] according to the following formula, which assumes the oxidation of two Fe(II) by one H_2O_2 molecule:

$$[H_2O_2] = \frac{[Fe(II)] - R[Fe(III)]}{2(R+1)} \quad (1)$$

where R is the target magnetite stoichiometry, and [Fe(III)] and [Fe(II)] are the initial concentrations in the stoichiometric magnetite suspension (mol L^{-1}). Then, resulting mineral suspension was magnetically separated and washed three times with ultrapure water, whose pH was adjusted to 8 with NaOH. The stoichiometry of all synthesized suspensions (Table S1) was measured by dissolving the synthesized magnetite nanoparticles in 5 M HCl, followed by Fe(II) content quantification by the 1,10-phenanthroline method.[26,27] Total Fe was measured after the reduction of Fe^{3+} by hydroxylamine hydrochloride. This synthesis approach has been demonstrated to be highly reproducible and produces pure magnetite phases without structural changes following controlled H_2O_2 treatments by wet chemistry, XRD, XAS, and XMCD studies by our group[17,25] and others.[14,21] Nominal R values and acid digestion results are generally in excellent agreement, except for R0.1, for which slightly higher value was measured (0.16 ± 0.01), which is due to the relatively higher stability of a small Fe(II)-rich core in nonstoichiometric magnetite nanoparticles.[22] This discrepancy has no importance for the present study because the objective of this study is to investigate a range of R values. The average particle diameter of the pristine magnetite was found equal to 11.5 ± 1.5 nm for R0.5, 10.6 ± 2.6 nm for R0.3, and 9.6 ± 2.6 nm for R0.1, by measuring 100 particles.[25] Assuming spherical particles, the surface area can be estimated around 100 m^2 g^{-1}.[17] After synthesis, the magnetite samples were properly stored in an anaerobic chamber in airtight bottles.

Sorption Experiments

Batch sorption experiments were conducted under anoxic conditions to measure the Cu sorption by magnetite nanoparticles. A 1000 mg L^{-1} Cu(II) stock solution was freshly prepared in Milli-Q water from $CuCl_2{\cdot}2H_2O$. Experiments systematically varied solution pH (4−9), magnetite stoichiometry (R0.1, R0.2, R0.3, R0.4, and R0.5), and initial Cu concentration ($[Cu]_{ini}$ = 25 and 500 μM), while background electrolyte concentration (10 mM NaCl) and total Fe concentrations 6.5 mM (equivalent to ∼0.5 g L^{-1} in case of stoichiometric magnetite) were set equal for all experiments. NaCl was selected as the background electrolyte (10 mM), because common alternative anions such as NO_3^- and ClO_4^- are oxidants that could interact with magnetite nanoparticles. Batch experiments were conducted in 50 mL polypropylene tubes. Dilute HCl and NaOH solutions were used to regularly adjust the solution pH to the desired values until the end of the experiments. After 1 month of reaction time, which was assumed to be enough to reach a steady state, the solid phase was separated from the liquid phase by magnetic separation. Then, the liquid phase was passed through 0.22 μm poly(ether sulfone) (PES) filter membranes (Sartorius Minisart). Aqueous Cu ($[Cu]_{aq}$) and Cu(II) ($[Cu(II]_{aq}$) concentrations were quantified using inductively coupled plasma mass spectrometry (ICP-MS) and a cupric ion-selective electrode (ISE), respectively. A quadrupole ICP-MS instrument (Agilent Technologies 7700X) was used. Before $[Cu]_{aq}$ quantification, calibration curves were performed and validated using certified material references (SLRS-6, National Research Council; Cu quantitative recovery ≥95%). A rhodium solution was used as an internal standard to correct for the instrumental drift and potential matrix effects. The limit of Cu quantification was determined to be 0.29 nM (18.59 ppt) (based on AFNOR specifications). $[Cu(II)]_{aq}$ in O_2 free solutions can reliably be derived from ISE measurements.[28,29] Detailed analysis procedure and calibration protocol are provided in Text S1 and Figure S1 in the Supporting Information.

XAS and XMCD

XAS and XMCD measurements were performed at the DEIMOS beamline (SOLEIL synchrotron).[30] A fraction of each sample was transported to the SOLEIL Synchrotron facility in 1 mL tubes and placed in airtight bottles that had been closed in the N_2-glovebox. At DEIMOS beamline, samples were handled in an Ar-glovebox (Jacomex $O_2(g) < 1$ ppm) that is connected to the experiments end station. Samples were prepared by dropping colloidal suspensions on silicon plates, which were dried at room temperature in the Ar-glovebox, then placed on a sample holder, which was transferred to the superconducting magnet as end-station. The XAS and XMCD spectra at Fe $L_{2,3}$ edges were recorded in total-electron-yield (TEY) detection mode, at 4.2 K within an ultrahigh vacuum environment (∼10^{-10} mbar). XAS spectra were recorded at Fe $L_{2,3}$ edges in the presence of a ±6 T magnetic induction. The circularly polarized X-rays were provided by an Apple-II HU52 undulator. The XMCD signals were recorded by flipping both the circular polarization (left and right helicity) and the external magnetic field (either H+ = +6.4 T or H− = −6.4 T). Each isotropic XAS spectra were plotted as the average $\sigma_{XAS} = (\sigma_+ + \sigma_-)/2$, while XMCD spectra were thereby acquired by taking the difference $\sigma_{XMCD} = (\sigma_+ - \sigma_-)$, where $\sigma_+ = [\sigma_L(H^-) + \sigma_R(H^+)]/2$ and $\sigma_- = [\sigma_L(H^+) + \sigma_R(H^-)]/2$. Under the same experimental conditions, XAS spectra at the Cu $L_{2,3}$-edges were

https://doi.org/10.1021/acsearthspacechem.5c00315
ACS Earth Space Chem. 2026, 10, 507−514

also collected without an external magnetic field. XAS measurements were performed on copper reference standards Cu(0), $Cu(OH)_2$, and CuOH. Pure Cu monocrystal was cleaned by Ar^+ bombardment under vacuum. $Cu(OH)_2$ was synthesized via NaOH-induced Cu^{2+} precipitation. CuOH was synthesized by using the same precipitation method with hydroxylamine addition to reduce Cu(II) to Cu(I). All spectra were background-subtracted and then normalized by their maximum values to enable quantitative comparison.

High-Resolution Transmission Electron Microscopy (HR-TEM)

Cu-magnetite nanoparticle samples were diluted with ultrapure water, and droplets were deposited on Cu-free holey carbon films supported on 200 mesh nickel microgrids (Oxford) and mounted on the sample holder in the N_2-glovebox. Sample had to be exposed to air only few seconds for the sample transfer to the instrument, as no better protocol could be found. HR-TEM images were acquired using a JEOL JEM 2100 LaB6 STEM microscope (80–200 kV) equipped with CCD cameras (Orius 200D, UltraScan 1000) and probe EDS (Oxford).

Geochemical Speciation Modeling

Aqueous chemical speciation calculations were performed using PhreePlot,[31] which contains an embedded version of the geochemical speciation program PHREEQC.[32] The "minteq v4" aqueous reaction database was used for the calculations in which ionic strength effects on equilibrium constants were calculated by using the Davies equation. Relevant reaction equations and constants to predict Cu speciation are summarized in Table S2. Redox potential values in magnetite suspensions were calculated versus pH and magnetite stoichiometry with PHREEQC, assuming a binary solid solution between maghemite and magnetite and by using the Guggenheim equation,[33] as described in previous studies.[20,22,25]

RESULTS AND DISCUSSION

Aqueous Cu Removal by Magnetite Nanoparticles

Cu removal from solution was studied in batch experiments on magnetite nanoparticles with varying stoichiometries (Nominal R = 0.1, 0.3, 0.5), pH (4–9), and initial Cu(II) concentrations ($[Cu]_{ini}$ = 500 and 25 μM). As shown in Figure 1a, a characteristic sigmoid pH sorption edge was observed regardless of $[Cu]_{ini}$. At pH 4, negligible Cu sorption occurred, followed by a sharp increase between pH 4 and 6, ultimately reaching almost complete removal at pH ≥7. This pH-dependent sorption behavior aligns with previously reported Cu(II) sorption patterns on iron oxyhydroxydes (e.g., goethite[7,34] or lepidocrocite[7]). By contrast with $[Cu]_{ini}$, magnetite stoichiometry significantly influenced Cu sorption, with stoichiometric magnetite demonstrating superior sorption compared to nonstoichiometric magnetite nanoparticles. These results are consistent with previous studies, in which it was reported enhanced Cu sorption onto magnetite with higher stoichiometry.[15,16]

Cu Redox Speciation in the Aqueous Phase

The redox speciation of Cu in aqueous solution is shown in the pH-Eh predominance (Pourbaix) diagram for $[Cu]_{ini}$ = 500 μM in 10 mM NaCl (Figure 1b). Precipitation reactions were excluded from these calculations to enable direct comparison with present experimental results, for which aqueous Cu redox speciation was determined following solid-phase separation.[35] The calculated Pourbaix diagram was overlaid with the theoretical redox conditions occurring in magnetite suspensions exhibiting $0.1 \leq R \leq 0.5$.[22] The thermodynamic calculations predict a distinct pH-dependent transition in Cu speciation under the redox conditions imposed by magnetite. Specifically, Cu(II) species dominate for pH < 5, while Cu(I) species (predominantly $CuCl_2^-$) become thermodynamically favored at pH > 5. Experimental validation of these theoretical predictions was achieved by using ISE measurements to quantify $[Cu(II)]_{aq}/[Cu(I)]_{aq}$ in solution following the interaction with nanomagnetites. Results confirmed that aqueous Cu predominantly existed as Cu(II) at pH <5 (i.e., $[Cu(II)]_{aq}/[Cu(I)]_{aq} > 1$), irrespective of $[Cu]_{ini}$ (Figure 1c and Figure S3, for 500 and 25 μM Cu, respectively). At pH >5, $[Cu(II)]_{aq}/[Cu(I)]_{aq}$ declined below unity, indicating Cu(I) prevalence across all magnetite stoichiometries investigated. The experimental data aligned relatively well with theoretical predictions of $[Cu(II)]_{aq}/[Cu(I)]_{aq}$, with model calculations capturing the Cu redox speciation trend semiquantitatively for pH >4.7. However, no significant effect of magnetite stoichiometry on aqueous Cu redox speciation was detected under the investigated conditions (Figure 1c). Indeed, for pH <6, comparable Eh values were measured in all magnetite suspensions for $0.1 \leq R \leq 0.5$ (Figure 1b),[22] and aqueous Cu was hardly detected at pH >6 because of its strong sorption.

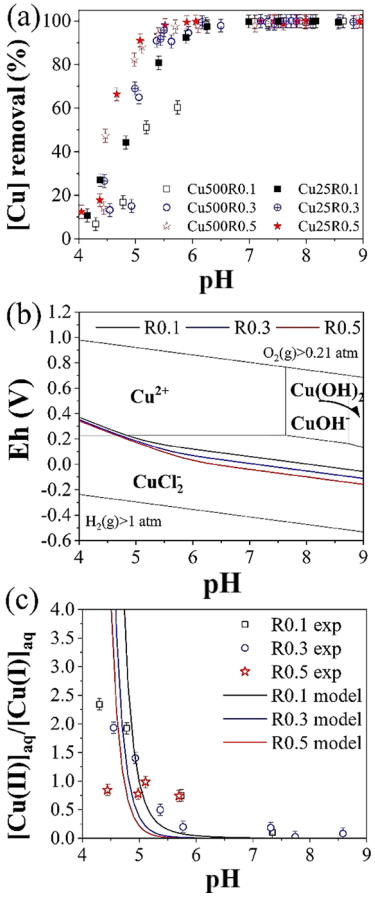

Figure 1. (a) Cu removal (%) from the aqueous phase versus pH (4–9), magnetite stoichiometries (R = 0.1, 0.3, 0.5) and $[Cu]_{ini}$ (500 and 25 μM), for total Fe concentrations of 6.5 mM in 10 mM NaCl. (b) Predominance pH-Eh (Pourbaix) diagram of Cu without considering precipitation ($[Cu]_{ini}$ = 500 μM, [NaCl] = 10 mM). Lines correspond to predicted redox conditions in magnetite suspensions for different stoichiometries.[22] (c) Experimental and modeled $[Cu(II)]_{aq}/[Cu(I)]_{aq}$ as a function of pH (4–9), magnetite stoichiometries (R = 0.1, 0.3, 0.5) for $[Cu]_{ini}$ = 500 μM. Lines correspond to predicted $[Cu(II)]_{aq}/[Cu(I)]_{aq}$ in magnetite suspensions for different stoichiometries.

https://doi.org/10.1021/acsearthspacechem.5c00315
ACS Earth Space Chem. 2026, 10, 507–514

Effect of Magnetite Stoichiometry on Cu Surface Redox Speciation

XAS at the Cu $L_{3,2}$ edges was employed to determine the redox speciation of Cu sorbed onto magnetite with different R values (0.1, 0.2, 0.3, 0.4, and 0.5) and $[Cu]_{ini}$ (25 and 500 μM) at pH 8 (Figure 2). Reference spectra for $Cu(OH)_2$, CuOH, and metallic Cu(0) are included for comparison, which matches well in both peak position and line shape with previously published reports.[36,37] For $[Cu]_{ini}$ = 25 μM on R0.1, the spectrum shows an L_3-edge peak at 927.4 eV and an L_2-edge peak at 947 eV, which matches well with the Cu(II) reference spectrum, indicating that Cu is sorbed in the Cu(II) form. As stoichiometry increases, the Cu(II) peak at 927.4 eV decreases while a new peak at 930 eV emerges, consistent with the Cu(I) reference, indicating a surface speciation shift from Cu(II) to Cu(I). At this low Cu concentration (25 μM), no significant Cu(0) formation was observed even with R0.5. At higher Cu concentration ($[Cu]_{ini}$ = 500 μM), the extent of Cu(II) reduction was substantially lower for R < 0.3, with only slight reduction occurred to Cu(I). However, for R0.5, the peak at 930 eV broadens and additional characteristic peaks appeared at ~934 and ~938 eV. HR-TEM micrographs and EDS analysis confirmed the occurrence of Cu-rich nanoparticles alongside magnetite nanoparticles (Figure S3), indicating Cu(0) nanoparticle formation.

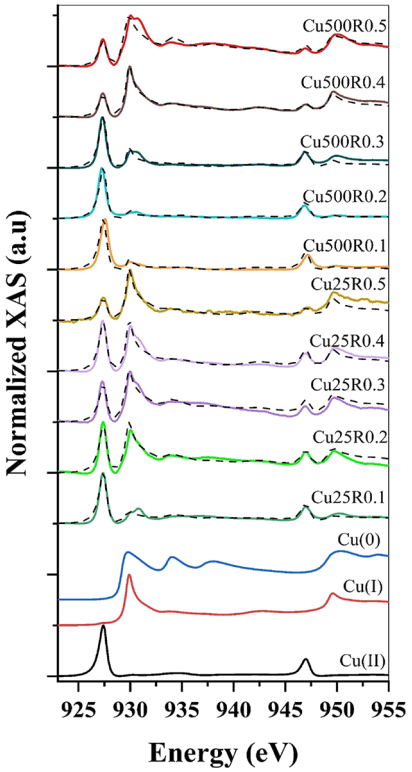

Figure 2. XAS at Cu $L_{3,2}$ edges (solid colored lines) and linear-combination fitting (dotted black lines) of Cu interacted with nanomagnetites (R = 0.1, 0.2, 0.3, 0.4, 0.5), for different $[Cu]_{ini}$ (25 and 500 μM) at pH 8. Reference spectra of $Cu(OH)_2$, CuOH, and metal Cu are shown for comparison.

To quantify the surface redox speciation of Cu, linear-combination fitting (LCF) of Cu $L_{2,3}$-edge XAS spectra was performed using Cu metal and Cu(II) and Cu(I) reference spectra. The result of the fit is shown in Figure 2. The fit was performed using Cu L_3-edge only (from 920.5 to 940 eV) because of its stronger intensity, better-defined peaks, and smaller sensitivity to background removal procedure than the L_2-edge, for which results are only simulated. For $[Cu]_{ini}$ = 25 μM, Cu surface redox speciation varied systematically from predominantly Cu(II) (82%) to Cu(I) (70%) with increasing magnetite stoichiometry (Figure 3a). For $[Cu]_{ini}$ = 500 μM, similar trends were observed for 0.1 ≤ R ≤ 0.4 (Figure 3b). The R0.1 surface retained predominantly Cu(II), consistent with $[Cu]_{ini}$ = 25 μM. The fraction of surface Cu(I) progressively increased across intermediate stoichiometries, from ~30% on R0.3 to ~70% on R0.4 surfaces. Notably, R0.5 exhibited a more complex oxidation-state distribution with nearly equivalent proportions of Cu(II), Cu(I), and Cu(0). These results demonstrate that R0.5 can drive Cu reduction to metallic Cu(0), but only at high $[Cu]_{ini}$ (500 μM, equivalent to ~32 mg L^{-1}), characteristic of severely contaminated mining sites (up to 200 mg L^{-1}).[38,39] This indicates that Cu(II) and Cu(I) surface species remain stable under most environmental conditions, with Cu(0) formation being limited to highly contaminated scenarios. The concentration-dependent formation of Cu(0) can be related to the degree of saturation in the aqueous phase, as illustrated by the larger stability field of Cu(0) at high $[Cu]_{aq}$ compared to low $[Cu]_{aq}$ in pH-Eh diagrams (Figure S4).

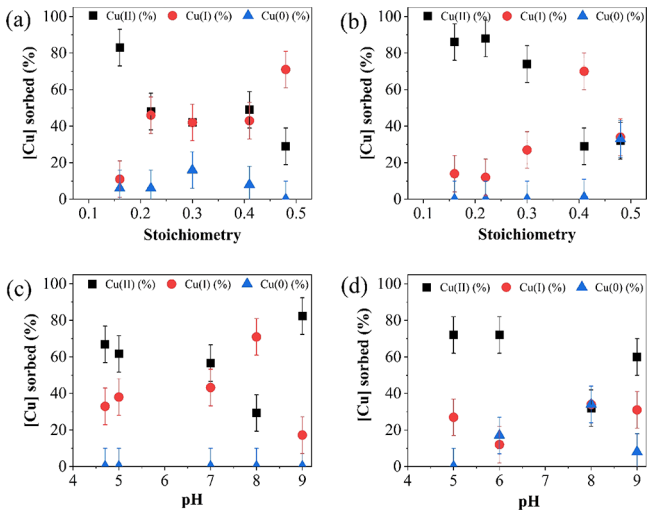

Figure 3. Linear-combination fit results of XAS. Oxidation-state distribution of Cu at pH 8 versus magnetite stoichiometry for (a) $[Cu]_{ini}$ = 25 μM and (b) $[Cu]_{ini}$ = 500 μM. Oxidation-state distribution of Cu on R0.5 versus pH for (c) $[Cu]_{ini}$ = 25 μM and (d) $[Cu]_{ini}$ = 500 μM.

Effect of pH on Cu Redox Speciation at the Surface of Stoichiometric Magnetite

The effects of pH (4–9) on Cu redox speciation at the R0.5 surface have also been investigated by XAS for both $[Cu]_{ini}$ (Figure S5). As similar features were observed in the spectra, the LCF procedure was applied to the Cu L_3-edge spectra for $[Cu]_{ini}$ = 25 μM (Figure 3c) and 500 μM (Figure 3d). For both $[Cu]_{ini}$, the fraction of surface Cu(II) is similar: it prevails (>80%) at low pH but its proportion relative to other oxidation states decreases down to ~30% at pH 8.

A particularly noteworthy finding emerged from comparison of Cu redox speciation distributions between sorbed (Figure 3c,d for $[Cu]_{ini}$ = 25 and 500 μM, respectively) and aqueous

https://doi.org/10.1021/acsearthspacechem.5c00315
ACS Earth Space Chem. 2026, 10, 507−514

phases (Figure S2 and Figure 1c for $[Cu]_{ini}$ = 25 and 500 μM, respectively). While Cu(I) prevails in the solution for pH >5, Cu(II) prevails at the R0.5 surface up to pH 7. This differential oxidation-state distribution between surface and solution, also observed for other redox-sensitive elements,[40−42] indicates that Cu(II) forms more stable species at the magnetite−water interface (e.g., surface incorporation, surface complexes, nanoclusters, or Cu(II) hydroxides precipitate), over Cu(I) species. This difference between solution and surface redox speciation is particularly striking at pH 9, where a strong Cu(II) surface stabilization is observed for both $[Cu]_{ini}$, which might arise from the formation of new surface species involving Cu(II) at high pH values, e.g., via the formation of ternary surface-Cu(II)−OH complexes, as observed on other Fe-oxides.[6]

The Cu(0) formation on the R0.5 surface depends on both pH and initial Cu concentration. At $[Cu]_{ini}$ = 25 μM, Cu(II) reduces only to Cu(I) across all pH values, with no Cu(0) detected (Figure 3c). At $[Cu]_{ini}$ = 500 μM, Cu(0) amounts for ∼20% of $[Cu]_{sorbed}$ at pH 6, increasing to ∼30% at pH 8 (Figure 3d). Thermodynamic pH-Eh predominance diagrams (Figure S4) predict enhanced reduction at high $[Cu]_{ini}$ but substantially overestimate Cu(0) formation. This discrepancy highlights a critical limitation of thermodynamic calculation omitting surface species, which strongly stabilizes Cu(II) and Cu(I) species and prevents further reduction to Cu(0). This also suggests that Cu redox speciation is mineral-specific and depends on both the reduction capacity of the mineral and distinct surface reactivities toward Cu(II) and Cu(I). For instance, the high Fe(II) content of green rust may provide exceptional reducing capacity, leading to complete reduction of Cu(II) to Cu(0).[11] By contrast, on the surface of pyrite, Cu(II) reduction proceeds to Cu(I), which has high affinity for reduced sulfur species, with only limited Cu(0) formation.[8,9] The present study shows that the magnetite surface stabilizes Cu(II) and Cu(I) species, with Cu(0) formation occurring only for high Cu surface loadings.

Effects of Cu(II) Reduction on Magnetite Stoichiometry

Cu(II) reduction to Cu(I) or Cu(0) is primarily controlled by structural Fe(II) (eq 2−3) thereby lowering Fe(II)/Fe(III), which can be probed by XMCD at Fe L_3-edge (Figure 4a):

$$Fe(II) + Cu(II) \rightarrow Fe(III) + Cu(I) \quad (2)$$

$$Fe(II) + Cu(I) \rightarrow Fe(III) + Cu(0) \quad (3)$$

The XMCD spectra of R0.5 at the Fe L_3-edge exhibit three main peaks: peak S1 at ∼712.9 eV corresponding to both Fe(II) and Fe(III) in octahedral (Oh) sites, but is dominated by Fe(II); peak S2 at ∼ 714.0 eV corresponding to the contribution of Fe(III) in tetrahedral (Td) sites; and peak S3 at ∼714.7 eV is attributed to Fe(III) in Oh sites.[43,44] Adding 25 μM Cu(II) leads to a XMCD spectrum very similar to that obtained for the R0.5 before reaction (Figure 4a), which suggests no significant difference in Fe redox speciation because of the small $[Cu]_{ini}$ relative to structural [Fe(II)]. By contrast, in the presence of 500 μM Cu, the diminished S1 peak intensity with a constant S3 peak intensity shows a significant effect of $[Cu]_{ini}$ on the redox speciation of Fe in magnetite. Similar observations were also made for the other stoichiometries (R0.1 to R0.4; see Figure S6). Note that in all spectra, Cu-nanomagnetite interaction induces subtle shifts in the L_3-edge energies to lower energy across all stoichiometries by <0.10 eV (Figure 4a and Figure S6), likely reflecting altered

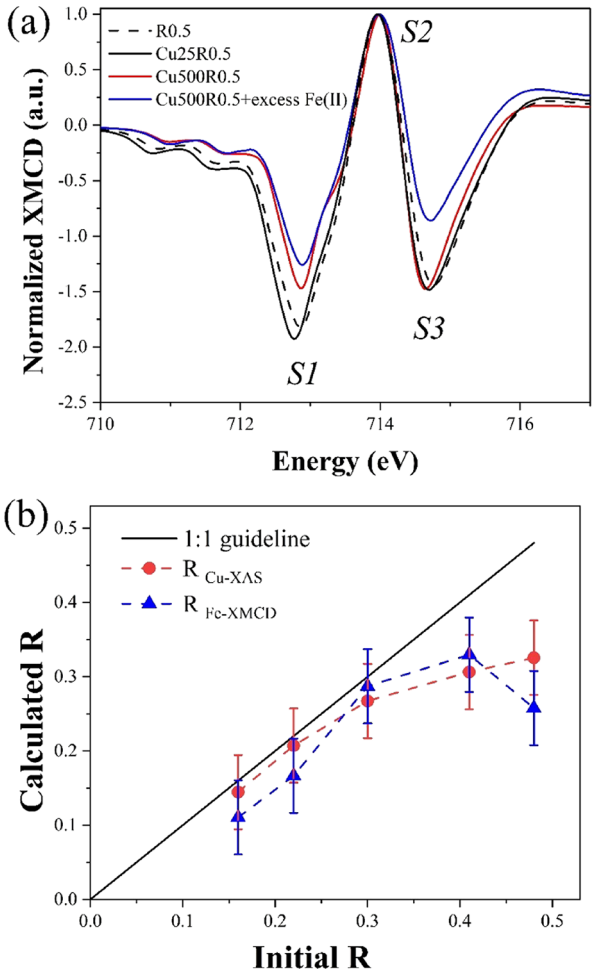

Figure 4. (a) Normalized XMCD spectra at the Fe L_3-edge of R0.5 interacted with 0, 25, or 500 μM Cu, or 500 μM Cu + 1 mM Fe(II), pH 8. (b) R values before (initial) and after reaction with Cu, as calculated from Cu L_3 XAS ($R_{Cu\text{-}XAS}$) and Fe XMCD ($R_{Fe\text{-}XMCD}$) for $[Cu]_{ini}$ = 500 μM.

local electronic environments around Fe centers,[43] though the specific mechanism requires further investigation.

The three XMCD peak intensities can be used to estimate the magnetite mole fraction (X) in nonstoichiometric magnetite. The evolution of peak intensities was monitored using the S indicator:

$$S = \frac{(S_1 + S_2)}{(S_2 + S_3)} \quad (4)$$

The S indicator was then used to calculate the mole fraction of magnetite in the magnetite−maghemite mixture (X), which can then be used to calculate R at the end of interaction ($R_{Fe\text{-}XMCD}$), according to the method described by Jungcharoen et *al.*:[17]

$$X = \frac{(S - 0.737)}{0.446} \quad (5)$$

In addition, magnetite stoichiometry can be determined with a fully independent method: according to eqs 2−3 using results of the LCF of Cu $L_{2,3}$-edge XAS data from Figure 3:

$$R_{Cu-XAS} = \frac{([Fe(II)] - [Cu(I)] - 2^*[Cu(0)])}{([Fe(III)] + [Cu(I)] + 2^*[Cu(0)])} \quad (6)$$

https://doi.org/10.1021/acsearthspacechem.5c00315
ACS Earth Space Chem. 2026, 10, 507−514

Uncertainty associated with $R_{Cu\text{-}XAS}$ was assumed to be equal to that determined previously for $R_{Fe\text{-}XMCD}$ (±0.05). Applications of eq 4−5 to pristine samples (R0.1 to R0.5) confirmed the consistence between nominal and measured stoichiometry using either acid digestion or XMCD results (Table S1; except for R0.1, for which slight discrepancies were previously explained). Accordingly, the initial R values determined by acid digestion were used for the calculations. Also note that as the samples were measured during the same synchrotron beamtime as the Cu-containing samples, this confirmed that potential O_2 contamination was successfully avoided during all experimental steps. For $[Cu]_{ini}$ = 25 μM and R0.5, 71% Cu(II) was reduced to Cu(I), so the electron demand (17.8 μM) represents only a minor fraction of the structural [Fe(II)] (0.8%), resulting in negligible difference in Fe(II)/Fe(III) (Figure 4a and Figure S7). Conversely, for $[Cu]_{ini}$ = 500 μM and R0.5, the electron demand (503.5 μM) approaches the same order of magnitude as the available Fe(II) electron equivalents (23.3%), leading to a measurable lowering of R. Figure 4b compares the results of $R_{Fe\text{-}XMCD}$ and $R_{Cu\text{-}XAS}$ at pH 8 and $[Cu]_{ini}$ = 500 μM versus initial R values. Both values agree well, which confirms that reactions 2−3 occurred and shows the consistency between the oxidation-state distribution of Cu and Fe determined by two distinct methods. After interacting magnetite with Cu(II), R values (i.e., $R_{Fe\text{-}XMCD}$ or $R_{Cu\text{-}XAS}$) remain unchanged for lower stoichiometries ($R \leq 0.3$), in agreement with the relatively small amounts of Cu(II) reduced, as observed by XAS (Figures 2a and 3b). For magnetite nanoparticles with higher stoichiometries (R0.4 and R0.5), where significant Cu(II) reduction occurs, R values decrease to approximately 0.3. Once the magnetite stoichiometry approaches $R \leq 0.3$, i.e., for $[Cu]_{ini}$ = 500 μM at pH 8, the remaining structural Fe(II) becomes inaccessible or energetically unfavorable for further redox reactions, establishing a threshold beyond which additional Cu(II) reduction becomes thermodynamically limited.

Enhanced Cu(II) Reduction through Fe(II) Amendment

Oxidized magnetite can be recharged to stoichiometric magnetite by adding aqueous Fe(II), which restores its redox properties.[14] This recharge process is rapid, enabling continuous regeneration when aqueous Fe(II) is present in excess during contaminant reduction.[45] To investigate the potential of achieving complete Cu(II) reduction to Cu(0), 1000 μM $[Fe(II)]_{aq}$ was added to an R0.5 suspension at pH 8 for 500 μM Cu. The Cu L_3 XAS analysis revealed that $Fe(II)_{aq}$ amendment significantly promoted Cu(0) formation to approximately 79%, with the remaining 21% persisting as Cu(II) (Figure 5). This demonstrates that excess Fe(II) drives Cu(I) reduction to metallic Cu(0), while Cu(II) surface species on magnetite remain stabilized due to the strong interaction of Cu with magnetite. These results contradict previous suggestions that stable Cu(I)-hydroxide surface complexes limit electron transfer and trap Cu in its + I oxidation state,[9] indicating that sufficient Fe(II) recharge can overcome this barrier to Cu(I) reduction.

XMCD analysis confirmed that Fe(II) amendment maintained magnetite stoichiometry, with $R_{Fe\text{-}XMCD}$ (using eq 5) and $R_{Cu\text{-}XAS}$ (using eq 6) approximately equal to 0.5 ($R_{Fe\text{-}XMCD}$ = 0.55 ± 0.05 and $R_{Cu\text{-}XAS}$ = 0.46 ± 0.05). Fe(II) amendment effectively recharges oxidized magnetite, helping to preserve magnetite stoichiometry and facilitating substantial Cu(II) reduction, in agreement with previous studies.[14,17,21,45] The

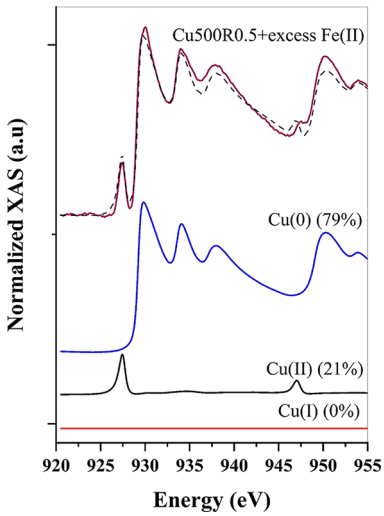

Figure 5. (a) XAS at Cu $L_{3,2}$ edges (solid colored lines) and linear-combination fitting (dotted black lines) of R0.5 interacted with 500 μM Cu + 1 mM Fe(II) at pH 8. The contributions (%) of Cu references to the sample spectrum are also shown below.

slightly hyperstoichiometric $R_{Fe\text{-}XMCD}$ (>0.5) indicates surface-localized Fe(II) enrichment consistent with previous $Fe(II)_{aq}$ recharge studies of magnetite.[21] Nevertheless, the normalized XMCD spectrum (Figure 4a) exhibits decreased S1 and S3 intensities relative to pure R0.5, indicating that Fe(II) recharge does not remove potential lattice-substituted Cu. The residual Cu (as substituted Cu(II) or reduced Cu(0) nanoparticles) introduces lattice strain and perturbs magnetic exchange,[46] enhancing spin canting and thereby lowering the net Fe magnetic moment. Thus, although oxidation-related defects are reversible by Fe(II) recharge, heterovalent dopant-induced lattice modification persists and suppresses XMCD intensity. Similar behavior has been reported in $Co_{1-x}Fe_{2+x}O_4$, where cation substitution and minor stoichiometric changes cause disproportionate magnetic moment changes via lattice distortion and enhanced spin canting, confirming that heterovalent dopants create persistent magnetic disorder not reversed by simple redox recharge.[47]

Environmental Implications

This study reveals new insights into Cu behavior in magnetite-bearing environments, with direct implications for contaminated site assessment and remediation strategies. The observed pH-dependent Cu(II)/Cu(I) aqueous speciation in magnetite suspensions validates existing geochemical models for predicting Cu mobility in natural systems. Cu(I), which exhibits substantially higher toxicity and bioavailability than Cu(II), occurs across most experimental conditions, representing a major environmental concern. At low Cu concentrations (25 μM, typical of moderately contaminated systems), magnetite promotes Cu(II) reduction to Cu(I) without Cu(0) formation, potentially increasing Cu toxicity. At high Cu concentrations (500 μM, characteristic of mining sites), limited Cu(0) formation occurs only under highly reducing conditions (R0.5, pH 8), while Cu(I) remains the dominant reduced species. Differential partitioning behavior between sorbed and aqueous Cu species reveals that Cu(II) exhibits greater surface binding affinity on R0.5 surfaces under both strongly acidic (pH <5) and alkaline (pH 9) conditions, while Cu(I) dominates in solution regardless of Cu loading. This suggests that naturally occurring magnetite in mine tailings, contami-

https://doi.org/10.1021/acsearthspacechem.5c00315
ACS Earth Space Chem. 2026, 10, 507−514

nated sediments, and industrial sites, can function as both a Cu(II) sink and Cu(I) producer, fundamentally altering Cu risk assessment in Fe-mineral-dominated systems. Magnetite stoichiometry controls Cu reduction capacity: at $R \leq 0.3$, structural Fe(II) sites become limiting for Cu(II) reduction. This stoichiometry dependence represents a previously unrecognized control on Cu speciation. However, the demonstrated ability of aqueous Fe(II) to recharge magnetite stoichiometry suggests that dynamic Fe cycling may facilitate Cu reduction. Moreover, engineered systems might consider Fe(II) amendment to maximize Cu(0) immobilization, particularly at sites with elevated Cu concentrations. Overall, these findings highlight the importance of incorporating magnetite stoichiometry into environmental Cu speciation models, to achieve adequate risk assessments and optimal remediation designs.

■ ASSOCIATED CONTENT

Data Availability Statement

Data will be made available upon request.

Supporting Information

The Supporting Information is available free of charge at https://pubs.acs.org/doi/10.1021/acsearthspacechem.5c00315.

Details on targeted and measured R values; copper speciation quantified by a cupric ion-selective electrode with calibration; model parameters and predominance pH-Eh (Pourbaix) diagram of Cu considering Cu-containing solid-phase formation; TEM and TEM-EDX characterization of R0.5 following Cu interaction; effect of pH on Cu $L_{3,2}$-edge XAS spectra with linear-combination fitting; normalized Fe L_3-edge XMCD spectra of R0.1-R0.4 following Cu interaction; comparison of $R_{Cu\text{-}XAS}$ and $R_{Fe\text{-}XMCD}$ for $[Cu]_{ini} = 25\ \mu M$ (PDF)

■ AUTHOR INFORMATION

Corresponding Author

Rémi MARSAC − *Université Paris Cité, Institut de physique du globe de Paris, CNRS, Paris F-75005, France;* orcid.org/0000-0002-3166-3988; Email: remi.marsac@cnrs.fr

Authors

Jaimy SCARIA − *Univ Rennes, CNRS, Géosciences Rennes − UMR 6118, Rennes F-35000, France*

Mathieu PÉDROT − *Univ Rennes, CNRS, Géosciences Rennes − UMR 6118, Rennes F-35000, France;* orcid.org/0000-0001-5215-3808

Laura FABLET − *Univ Rennes, CNRS, Géosciences Rennes − UMR 6118, Rennes F-35000, France*

Fadi CHOUEIKANI − *Synchrotron SOLEIL, Saint-Aubin 91190, France*

Anne-Catherine PIERSON-WICKMANN − *Univ Rennes, CNRS, Géosciences Rennes − UMR 6118, Rennes F-35000, France*

Aline DIA − *Univ Rennes, CNRS, Géosciences Rennes − UMR 6118, Rennes F-35000, France*

Yann SIVRY − *Université Paris Cité, Institut de physique du globe de Paris, CNRS, Paris F-75005, France;* orcid.org/0000-0001-5431-1195

Charlotte CATROUILLET − *Université Paris Cité, Institut de physique du globe de Paris, CNRS, Paris F-75005, France*

Complete contact information is available at: https://pubs.acs.org/10.1021/acsearthspacechem.5c00315

Notes

The authors declare no competing financial interest.

■ ACKNOWLEDGMENTS

This work was supported by the COLOSSAL project funded by ANR (project number ANR-23-CE01-0001; PI: R.M.), the French Brittany Region (SAD project COLORED and ARED project NANOMAG) and the MADMAG project funded by the CNRS-INSU EC2CO program. The authors acknowledge the SOLEIL synchrotron for beamtime allocation at the DEIMOS beamline (proposals 20240217 and 20230086). Through the support of the GeOHeLiS analytical platform of Rennes University, this publication is also supported by the European Union through the European Regional Development Fund (FEDER), the French Ministry of Higher Education and Research, the French Region of Brittany and Rennes Metropole. The authors are grateful to L. Dutruch and M. Pattier for assistance in ICP-MS analysis, and V. Dorcet and L. Rault for assistance in TEM experiments performed on the THEMIS platform (ScanMAT, UMS 2011 University of Rennes-CNRS; CPER-FEDER 2007−2014).

■ REFERENCES

(1) Maharaj, P. P. P.; Barrett, P. M.; Ellwood, M. J. Biogeochemical Cycling of Dissolved Cu along the East Australian Current. *Mar. Chem.* **2025**, *268*, No. 104481.

(2) Gaetke, L. Copper Toxicity, Oxidative Stress, and Antioxidant Nutrients. *Toxicology* **2003**, *189* (1−2), 147−163.

(3) Gui, W.; Wang, W.-X. Intestinal Cu(II)/(I) Redox State Transformation Causes Cu(I) Overflow and Toxicity of the Gut and Liver in Zebrafish. *Environ. Sci. Technol.* **2025**, *59* (15), 7495−7505.

(4) Borch, T.; Kretzschmar, R.; Kappler, A.; Cappellen, P. V.; Ginder-Vogel, M.; Voegelin, A.; Campbell, K. Biogeochemical Redox Processes and Their Impact on Contaminant Dynamics. *Environ. Sci. Technol.* **2010**, *44* (1), 15−23.

(5) Huang, J.; Jones, A.; Waite, T. D.; Chen, Y.; Huang, X.; Rosso, K. M.; Kappler, A.; Mansor, M.; Tratnyek, P. G.; Zhang, H. Fe(II) Redox Chemistry in the Environment. *Chem. Rev.* **2021**, *121* (13), 8161−8233.

(6) Bochatay, L.; Persson, P.; Lövgren, L.; Brown, G. E. XAFS Study of Cu(II) at the Water-Goethite (α-FeOOH) Interface. *J. Phys. IV* **1997**, *7* (C2), C2-819−C2−820.

(7) Peacock, C. L.; Sherman, D. M. Copper(II) Sorption onto Goethite, Hematite and Lepidocrocite: A Surface Complexation Model Based on Ab Initio Molecular Geometries and EXAFS Spectroscopy. *Geochim. Cosmochim. Acta* **2004**, *68* (12), 2623−2637.

(8) Voigt, S.; Szargan, R.; Suoninen, E. Interaction of Copper(II) Ions with Pyrite and Its Influence on Ethyl Xanthate Adsorption. *Surf. Interface Anal.* **1994**, *21* (8), 526−536.

(9) Weisener, C.; Gerson, A. Cu(II) Adsorption Mechanism on Pyrite: An XAFS and XPS Study. *Surf. Interface Anal.* **2000**, *30* (1), 454−458.

(10) Markl, G.; Bucher, K. Reduction of Cu2+ in Mine Waters by Hydrolysis of Ferrous Sheet Silicates. *Eur. J. Mineral.* **1997**, *9* (6), 1227−1236.

(11) O'Loughlin, E. J.; Kelly, S. D.; Kemner, K. M.; Csencsits, R.; Cook, R. E. Reduction of AgI, AuIII, CuII, and HgII by FeII/FeIII Hydroxysulfate Green Rust. *Chemosphere* **2003**, *53* (5), 437−446.

(12) Chen, J.; Zhou, X.; Zhu, Y.; Zhang, Y.; Huang, C.-H. Synergistic Activation of Peroxydisulfate with Magnetite and Copper Ion at Neutral Condition. *Water Res.* **2020**, *186*, No. 116371.
(13) White, A. F.; Peterson, M. L. Reduction of Aqueous Transition Metal Species on the Surfaces of Fe(II) -Containing Oxides. *Geochim. Cosmochim. Acta* **1996**, *60* (20), 3799−3814.
(14) Gorski, C. A.; Nurmi, J. T.; Tratnyek, P. G.; Hofstetter, T. B.; Scherer, M. M. Redox Behavior of Magnetite: Implications for Contaminant Reduction. *Environ. Sci. Technol.* **2010**, *44* (1), 55−60.
(15) Bayer, T.; Wei, R.; Kappler, A.; Byrne, J. M. Cu(II) and Cd(II) Removal Efficiency of Microbially Redox-Activated Magnetite Nanoparticles. *ACS Earth Space Chem.* **2023**, *7* (10), 1837−1847.
(16) Demangeat, E.; Pédrot, M.; Dia, A.; Bouhnik-Le-Coz, M.; Davranche, M.; Cabello-Hurtado, F. Surface Modifications at the Oxide/Water Interface: Implications for Cu Binding, Solution Chemistry and Chemical Stability of Iron Oxide Nanoparticles. *Environ. Pollut.* **2020**, *257*, No. 113626.
(17) Jungcharoen, P.; Pédrot, M.; Choueikani, F.; Pasturel, M.; Hanna, K.; Heberling, F.; Tesfa, M.; Marsac, R. Probing the Effects of Redox Conditions and Dissolved Fe $^{2+}$ on Nanomagnetite Stoichiometry by Wet Chemistry, XRD, XAS and XMCD. *Environ. Sci. Nano* **2021**, *8* (7), 2098−2107.
(18) Latta, D. E.; Gorski, C. A.; Boyanov, M. I.; O'Loughlin, E. J.; Kemner, K. M.; Scherer, M. M. Influence of Magnetite Stoichiometry on U^{VI} Reduction. *Environ. Sci. Technol.* **2012**, *46* (2), 778−786.
(19) O'Loughlin, E. J.; Boyanov, M. I.; Kemner, K. M. Reduction of Vanadium(V) by Iron(II)-Bearing Minerals. *Minerals* **2021**, *11* (3), 316.
(20) Scaria, J.; Pédrot, M.; Fablet, L.; Yomogida, T.; Nguyen, T. T.; Sivry, Y.; Catrouillet, C.; Pradas Del Real, A. E.; Choueikani, F.; Vantelon, D.; Dia, A.; Groleau, A.; Marsac, R. Magnetite Stoichiometry (Fe(II)/Fe(III)) Controls on Trivalent Chromium Surface Speciation. *Environ. Sci. Technol.* **2025**, *59* (11), 5747−5755.
(21) Ding, R.; Guida, C.; Pearce, C. I.; Arenholz, E.; Grenèche, J. M.; Gloter, A.; Scheinost, A. C.; Kvashnina, K. O.; Wang, K.; Fernandez-Martinez, A.; Mu, Y.; Rosso, K. M.; Charlet, L. Single Rhenium Atoms on Nanomagnetite: Probing the Recharge Process That Controls the Fate of Rhenium in the Environment. *Sci. Adv.* **2025**, *11* (20), No. eadq3650.
(22) Jungcharoen, P.; Pédrot, M.; Heberling, F.; Hanna, K.; Choueikani, F.; Catrouillet, C.; Dia, A.; Marsac, R. Prediction of Nanomagnetite Stoichiometry (Fe(II)/Fe(III)) under Contrasting pH and Redox Conditions. *Environ. Sci. Nano* **2022**, *9* (7), 2363−2371.
(23) Jungcharoen, P.; Marsac, R.; Choueikani, F.; Masson, D.; Pédrot, M. Influence of Organic Ligands on the Stoichiometry of Magnetite Nanoparticles. *Nanoscale Adv.* **2023**, *5* (16), 4213−4223.
(24) Byrne, J. M.; Klueglein, N.; Pearce, C.; Rosso, K. M.; Appel, E.; Kappler, A. Redox Cycling of Fe(II) and Fe(III) in Magnetite by Fe-Metabolizing Bacteria. *Science* **2015**, *347* (6229), 1473−1476.
(25) Fablet, L.; Choueikani, F.; Pédrot, M.; Marsac, R. What Are the Effects of Environmental Factors on Co Speciation at the Magnetite Surface? *Environ. Sci. Nano* **2024**, *11* (5), 2036−2048.
(26) Fortune, W. B.; Mellon, M. G. Determination of Iron with O-Phenanthroline: A Spectrophotometric Study. *Ind. Eng. Chem. Anal. Ed.* **1938**, *10* (2), 60−64.
(27) Tamura, H.; Goto, K.; Yotsuyanagi, T.; Nagayama, M. Spectrophotometric Determination of Iron(II) with 1,10-Phenanthroline in the Presence of Large Amounts of Iron(III). *Talanta* **1974**, *21* (4), 314−318.
(28) Maurer, F.; Christl, I.; Fulda, B.; Voegelin, A.; Kretzschmar, R. Copper Redox Transformation and Complexation by Reduced and Oxidized Soil Humic Acid. 2. Potentiometric Titrations and Dialysis Cell Experiments. *Environ. Sci. Technol.* **2013**, *47* (19), 10912−10921.
(29) Rivera-Duarte, I.; Zirino, A. Response of the Cu(II) Ion Selective Electrode to Cu Titration in Artificial and Natural Shore Seawater and in the Measurement of the Cu Complexation Capacity. *Environ. Sci. Technol.* **2004**, *38* (11), 3139−3147.
(30) Ohresser, P.; Otero, E.; Choueikani, F.; Chen, K.; Stanescu, S.; Deschamps, F.; Moreno, T.; Polack, F.; Lagarde, B.; Daguerre, J.-P.; Marteau, F.; Scheurer, F.; Joly, L.; Kappler, J.-P.; Muller, B.; Bunau, O.; Sainctavit, Ph. DEIMOS: A Beamline Dedicated to Dichroism Measurements in the 350−2500 eV Energy Range. *Rev. Sci. Instrum.* **2014**, *85* (1), No. 013106.
(31) Kinniburgh, D. G., Cooper, D. M.. *PhreePlot: Creating Graphical Output with PHREEQC*; 2011. http://www.phreeplot.org/ (accessed 2020−04−25).
(32) Parkhurst, D. L.; Appelo, C. A. J. *User's Guide to PHREEQC (Version 2): A Computer Program for Speciation, Batch-Reaction, One-Dimensional Transport, and Inverse Geochemical Calculations*; 1999. .
(33) Glynn, P. Solid-Solution Solubilities and Thermodynamics: Sulfates, Carbonates and Halides. *Rev. Mineral. Geochem.* **2000**, *40* (1), 481−511.
(34) Buerge-Weirich, D.; Hari, R.; Xue, H.; Behra, P.; Sigg, L. Adsorption of Cu, Cd, and Ni on Goethite in the Presence of Natural Groundwater Ligands. *Environ. Sci. Technol.* **2002**, *36* (3), 328−336.
(35) Kölling, M. Comparison of Different Methods for Redox Potential Determination in Natural Waters. In *Redox*; Schüring, J., Schulz, H. D., Fischer, W. R., Böttcher, J., Duijnisveld, W. H. M., Eds.; Springer Berlin Heidelberg: Berlin, Heidelberg, 2000; pp 42−54. .
(36) Grioni, M.; Goedkoop, J. B.; Schoorl, R.; De Groot, F. M. F.; Fuggle, J. C.; Schäfers, F.; Koch, E. E.; Rossi, G.; Esteva, J.-M.; Karnatak, R. C. Studies of Copper Valence States with Cu L 3 X-Ray-Absorption Spectroscopy. *Phys. Rev. B* **1989**, *39* (3), 1541−1545.
(37) Jiang, W.; Pelaez, M.; Dionysiou, D. D.; Entezari, M. H.; Tsoutsou, D.; O'Shea, K. Chromium(VI) Removal by Maghemite Nanoparticles. *Chem. Eng. J.* **2013**, *222*, 527−533.
(38) B.C. Ministry of Environment and Climate Change Strategy. *Copper Water Quality Guideline for the Protection of Freshwater Aquatic Life-Technical Report*; **2019**.
(39) Grosell, M. Homeostasis and Toxicology of Essential Metals. In *Copper; Fish Physiology*; Academic Press: London, 2012; *Vol. 31A*, pp 53−133.
(40) Marsac, R.; Catrouillet, C.; Pédrot, M.; Benedetti, M. F.; Dia, A.; Van Hullebusch, E. D.; Davranche, M.; Sivry, Y.; Pierson-Wickmann, A.-C.; Tharaud, M.; Heberling, F. Equilibrium Surface Complexation Modeling with Metastable Natural Colloids: The Key to Predict the Oxidation State Distribution of Trace Elements? *Curr. Opin. Colloid Interface Sci.* **2024**, *72*, No. 101820.
(41) Marsac, R.; Banik, N. L.; Lützenkirchen, J.; Buda, R. A.; Kratz, J. V.; Marquardt, C. M. Modeling Plutonium Sorption to Kaolinite: Accounting for Redox Equilibria and the Stability of Surface Species. *Chem. Geol.* **2015**, *400*, 1−10.
(42) Ratié, G.; Zhang, K.; Iqbal, M.; Vantelon, D.; Mahé, F.; Rivard, C.; Komárek, M.; Bouhnik-Le Coz, M.; Dia, A.; Hanna, K.; Davranche, M.; Marsac, R. Driving Forces of Ce(III) Oxidation to Ce(IV) onto Goethite. *Chem. Geol.* **2023**, *633*, No. 121547.
(43) Kowalska, J. K.; Nayyar, B.; Rees, J. A.; Schiewer, C. E.; Lee, S. C.; Kovacs, J. A.; Meyer, F.; Weyhermüller, T.; Otero, E.; DeBeer, S. Iron L2,3 -Edge X-Ray Absorption and X-Ray Magnetic Circular Dichroism Studies of Molecular Iron Complexes with Relevance to the FeMoco and FeVco Active Sites of Nitrogenase. *Inorg. Chem.* **2017**, *56* (14), 8147−8158.
(44) Pearce, C. I. Direct Determination of Cation Site Occupancies in Natural Ferrite Spinels by L2,3 X-Ray Absorption Spectroscopy and X-Ray Magnetic Circular Dichroism. *Am. Mineral.* **2006**, *91* (5−6), 880−893.
(45) Marsac, R.; Pasturel, M.; Hanna, K. Reduction Kinetics of Nitroaromatic Compounds by Titanium-Substituted Magnetite. *J. Phys. Chem. C* **2017**, *121* (21), 11399−11406.
(46) Suneetha, T.; Rao, G. N.; Ramesh, T. Structural, Vibrational and Magnetic Properties of Cu-Substituted Mn0.5Zn0.5Fe2O4 Nanoparticles. *J. Mater. Sci. Mater. Electron.* **2021**, *32* (11), 14420−14436.
(47) Moyer, J. A.; Vaz, C. A. F.; Arena, D. A.; Kumah, D.; Negusse, E.; Henrich, V. E. Magnetic Structure of Fe-Doped CoFe 2 O 4 Probed by x-Ray Magnetic Spectroscopies. *Phys. Rev. B* **2011**, *84* (5), No. 054447.